arXiv:2409.16990v3 [cs.CV] 9 Mar 2026

Graphical Abstract

Single Image, Any Face: Generalisable 3D Face Generation

Wenqing Wang, Haosen Yang, Josef Kittler, Xiatian Zhu *

The creation of 3D human face avatars from a single unconstrained image is a fundamental task that underlies numerous real-world vision and graphics applications. Despite the significant progress made in generative models, existing methods are either less suited in design for human faces or fail to generalise from the restrictive training domain to unconstrained facial images. To address these limitations, we propose a novel model, **Gen3D-Face**, which generates 3D human faces with unconstrained single image input within a multi-view consistent diffusion framework. Given a specific input image, our model first produces multi-view images, followed by neural surface construction. To incorporate face geometry information while preserving generalisation to in-the-wild inputs, we estimate a subject-specific mesh directly from the input image, enabling training and evaluation without ground-truth 3D supervision. Importantly, we introduce a multi-view joint generation scheme to enhance the appearance consistency among different views. To the best of our knowledge, this is the first attempt and benchmark for creating photorealistic 3D human face avatars from single images for generic human subject across domains. Extensive experiments demonstrate the superiority of our method over previous alternatives for out-of-domain single image 3D face generation and the top ranking competition for the in-domain setting.

*Corresponding author.

Highlights

Single Image, Any Face: Generalisable 3D Face Generation

Wenqing Wang, Haosen Yang, Josef Kittler, Xiatian Zhu [†]

- We investigate the under-studied single-image 3D face generation problem with a particular focus on the developed model ability to generalise to unconstrained unseen face imagery so that it is more practically useful and deployable. To the best of our knowledge, this is the very first attempt at tackling this meaningful problem setting in the single image 3D face generation framework with multi-view diffusion model.
- We propose Gen3D-Face, a novel framework that combines input-conditioned mesh estimation (providing geometric guidance without requiring ground-truth meshes) and joint multi-view diffusion generation (ensuring identity-preserving cross-view consistency), supported by a hybrid real-and-synthetic training strategy that improves robustness in out-of-domain scenarios.
- Extensive evaluations demonstrate that our method achieves state-of-the-art performance while offering practical advantages in scalability and applicability to unconstrained real-world single-image inputs, since it removes the need for specialised multi-view capture or ground-truth mesh supervision.

[†]Corresponding author.

Single Image, Any Face: Generalisable 3D Face Generation

Wenqing Wang[a], Haosen Yang[a], Josef Kittler[a], Xiatian Zhu [*a]

[a] *Centre for Vision, Speech and Signal Processing, University of Surrey, United Kingdom*

Abstract

The creation of 3D human face avatars from a single unconstrained image is a fundamental task that underlies numerous real-world vision and graphics applications. Despite the significant progress made in generative models, existing methods are either less suited in design for human faces or fail to generalise from the restrictive training domain to unconstrained facial images. To address these limitations, we propose a novel model, **Gen3D-Face**, which generates 3D human faces with unconstrained single image input within a multi-view consistent diffusion framework. Given a specific input image, our model first produces multi-view images, followed by neural surface construction. To incorporate face geometry information while preserving generalisation to in-the-wild inputs, we estimate a subject-specific mesh directly from the input image, enabling training and evaluation without ground-truth 3D supervision. Importantly, we introduce a multi-view joint generation scheme to enhance the appearance consistency among different views. To the best of our knowledge, this is the first attempt and benchmark for creating photorealistic 3D human face avatars from single images for generic human subject across domains. Extensive experiments demonstrate the efficacy and superiority of our method over previous alternatives for out-of-domain single image 3D face generation and the top ranking competition for the in-domain setting. Our code and dataset will be released upon acceptance.

Keywords: 3D Head Generation, Multi-view Diffusion, Novel View Synthesis

Figure 1: 3D human face avatar from (a) a single unconstrained image by (c) prior state-of-the-art model [1] (note the hallucinated hat and clear identity shift), vs. (d) our model.

1. Introduction

Generate photorealistic 3D face avatars is crucial for a wide range of real-world applications in computer graphics and computer vision, including video conferencing, virtual modeling, entertainment, and augmented or enhanced reality [2, 3, 4]. Existing 3D face modeling approaches predominantly rely on either multi-view image or video inputs [5, 6, 7, 8] or text-guided 3D generation [9, 10], each presenting inherent limitations. Multi-view reconstruction methods [5, 6, 7, 8] require calibrated multi-view captures and often involve costly per-identity optimization, restricting their applicability in practical scenarios where such input data is unavailable. On the other hand, text-guided avatar generation [9, 10] struggles to ensure identity authenticity and preserve fine-grained facial details, as human identity characteristics are difficult to accurately express through text descriptions alone. These constraints collectively highlight the need for a more accessible and identity-faithful solution to 3D face avatar generation.

Inspired by the remarkable success of generative diffusion models [11] and driven by the aforementioned challenges, *single-image 3D face generation* has become a trendy topic with the key challenges being the tasks of figuring out both geometry and appearance information from only a single face image of a generic human identity. These seemingly impossible tasks now become hopeful for two reasons: *The first* lies

*Corresponding author.

in the availability of unprecedentedly rich and comprehensive knowledge captured by off-the-shelf generative models, providing a chance of extracting and transferring useful information for particular downstream tasks (human face in this work) [12, 13]. For example, Stable Diffusion was trained with a massive (unknown) text-image pairs from the Internet, including a diversity of facial images from a broad range of subjects like celebrities. *The second* is the enormous technical advance in multi-view image generation [14, 15], 3D object representation, reconstruction, and generation [16, 17, 18]. Combining all these building blocks together properly could be the basis of plausible solutions to tackling this challenge.

Building on the pillars discussed above, an intuitive approach is to learn a generic 3D face generation model from a large, diverse collection of data with multi-view images per human identity, so that the model could generalize to generic unseen single face images. There are some early attempts pursuing this strategy by training on large synthetic digital avatars created by 3D artists [19]. This however raises the synthetic to real domain generalisation challenge, resulting in unrealistic face generation. Besides, the collection of human face data is much more restricted, due to both the intrinsic complexity and diversity, as well as the intricate privacy considerations. As a result, existing 3D face benchmarks are often limited in size and diversity in practice, e.g., containing only a few hundred identities [20, 21], making them insufficient for model training.

To mitigate this data scarcity challenge, the latest attempt for single-image 3D face generation leverages the human geometric priors by incorporating ground-truth mesh in multi-view synthesis [1]. A promising finding from this work is that properly blending image appearance and mesh's geometric knowledge enables the model to work across different views, producing good quality outputs. However, we find that their method suffers from several limitations that significantly hamper its generalisation to unconstrained face images shown in Figure 1: (i) *Overfitting to the training domain* due to the stringent need for training data. The limited data availability prevents the model to generalise to different unseen styles; (ii) *Over reliance on the ground-truth mesh*, which is often unavailable in practice; (iii) *Insufficient multi-view consistency* because of multi-view information does not communicate inside Unet Encoder.

In this work, to tackle this objective, we develop **Gen3D-Face**, a latent diffusion framework that jointly generates multi-view consistent images and leverages input-estimated face geometry along with hybrid real-and-synthetic training data to reconstruct photorealistic and generalisable 3D face avatars from a single unconstrained image. Our model first generates consistent multi-view face images and then conducts the neural surface construction. To enhance the data diversity, we generate synthetic 3D face images with off-the-shelf model [22]. Unlike prior diffusion-based avatar models that rely on ground-truth 3D head scans, which are expensive to obtain and raise privacy concerns, we exploit input-conditioned mesh estimation for not only mitigating the model's over reliance on the geometric prior, but also enabling it to generalise to typical cases without the ground-truth mesh, and with distinct appearance styles. To ensure multi-view consistency, we introduce a multi-view joint generation scheme.

Our **contributions** are summarised as follows: **(1)** We investigate the under-studied single-image 3D face generation problem with a particular focus on the developed model ability to generalise to unconstrained unseen face imagery so that it is more practically useful and deployable. To the best of our knowledge, this is the very first attempt at tackling this meaningful problem setting in the single image 3D face generation framework with multi-view diffusion model. **(2)** We propose Gen3D-Face, a novel framework that combines input-conditioned mesh estimation (providing geometric guidance without requiring ground-truth meshes) and joint multi-view diffusion generation (ensuring identity-preserving cross-view consistency), supported by a hybrid real-and-synthetic training strategy that improves robustness in out-of-domain scenarios. **(3)** Extensive evaluations demonstrate that our method achieves state-of-the-art performance while offering practical advantages in scalability and applicability to unconstrained real-world single-image inputs, since it removes the need for specialised multi-view capture or ground-truth mesh supervision.

2. Related Work

Novel view synthesis Neural fields [16] and 3D Gaussian Splatting [18] have emerged as the most effective 3D object and scene representations, capable of producing photo-

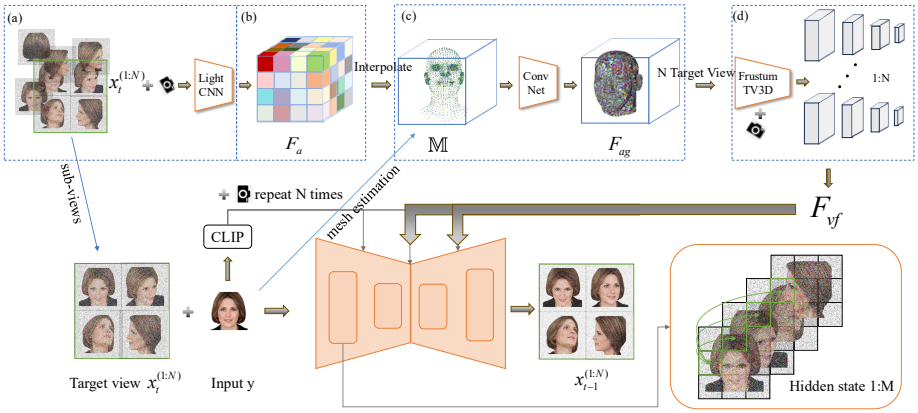

Figure 2: **An overview of our Gen3D-Face**. It adopts the latent diffusion paradigm involving the learning of multi-step denoising. Each step denoises N novel views conditioned on a single face image y and the mesh $\mathbb{M}$ estimated from y, following the process outlined as below: (a) A light CNN encoder is used to integrate the noise multi-view images $\mathbf{x}_t^{(1:N)}$ generated in the previous steps with camera angles and time embedding; (b) Its output is interpolated with a predefined 3D voxel to obtain the *appearance feature volume* F_a; (c) Combining F_a with the geometry prior $\mathbb{M}$ yields the *hybrid feature volume* F_{ag}; (d) Finally, the denoised views $\mathbf{x}_{t-1}^{(1:N)}$ are obtained by injecting F_{ag} to FrustumTV3DNet to obtain view frustum volume F_{vf}, which is fed into the diffusion backbone as the conditioning signal. Additionally, a CLIP-extracted global feature of the input image y is fused with the camera embedding of each target view, yielding N view-specific conditioning vectors that guide the multi-view diffusion process.

realistic images from arbitrary novel views of a scene. However, the first generation is reconstruction-based, necessitating densely captured views. To relax this assumption, follow-up approaches [23, 24] propose learning-based methods that require only a few views, utilizing scene priors from other existing datasets [23], or explicitly mapping the input image to a 3D Gaussian per pixel [24]. Commonly, these methods tend to be restricted to reconstructing relatively simple objects or confined to low resolution, due to their limited expressive capacity.

3D avatars from a single image In addition to reconstruction techniques, various methods have been developed to generate 3D avatars using Generative Adversarial Networks (GANs) [25, 22] or, more recently, diffusion models [11]. 3D-aware GANs learn 3D representation by integrating tri-planes [25] or tri-grids [22] combined with

the camera position. To achieve a single image 3D avatar generation, typically, GAN inversion is required to fit the input image, which is computationally expensive and time-consuming. Live3D [2] trains an image-to-triplane encoder to map an input image to a canonical triplane 3D representation instead of GAN inversion, while being still limited to large output angles. On the other hand, diffusion methods specifically designed for human avatars suffer from limited training data, as a 3D diffusion model is hard to learn from 2D image collections. For example, Morphable Diffusion [1] relies on pretrained 3D-aware diffusion models [11, 13] and incorporates 3D physical constraints [26] (ground-truth bilinear head meshes), while being trained on a relatively small and in-domain dataset. These restrictions limit its ability to generalise to unconstrained face images and requires specialised 3D acquisition. In this work, we tackle these challenges with a proper model design and data synthesis.

Multi-view diffusion models Recent works [13, 15, 14] extend 2D diffusion models to generate consistent multi-view images from a single-view. Their success benefits from the existence of large-scale 3D datasets [27]. For example, SyncDreamer [11], is a generic multi-view diffusion model trained on large 3D object datasets without a face-specific geometric prior, leading to weaker identity preservation on human faces. Extending along this direction, our work focuses on human face avatar generation with a special requirement on the model's ability to generalise to unconstrained imagery.

Learning from synthetic data Synthetic photorealistic data is effective in handling data scarcity. Recent methods have been developed to utilise synthetic data, either explicitly [28, 29] or implicitly [2], to enhance their performance in generative tasks. Portrait4D [29] focus more on motion-driven reenactment in the limited poses. The Gaussian Splatting method [28] needs per-identity optimization. In this work, we extend and validate this generic idea for the more challenging single image 3D face generation in unconstrained settings for a full 360°.

3. Method

Given a single face image y as input, we aim to generate a 3D face avatar for this person. To that end, we propose a new latent diffusion approach, **Gen3D-Face**, with

the architecture depicted in Figure 2. It generates consistent multi-view images from a single face image, which can then be fed into existing neural surface construction methods (e.g., Neus2[17]). For the former, we adopt the off-the-shelf Stable Diffusion [11] as the backbone, where the diffusion and denoising take place in a latent feature embedding space (e.g., a pretrained VAE). For the sake of being self-contained, we first briefly describe 2D and 3D diffusion.

3.1. Preliminaries: 2D and 3D Diffusion

Diffusion models [11] aim to gradually generate structured outputs of a target distribution from random noise through learning an iterative denoising model. Given a noise input x_t, where $t \in (0, T)$ denotes the step index with a total number of steps T, the model is trained to predict the added noise. If this noise is removed, a less noisy version x_{t-1} can be unveiled. Whilst these models can generate images of novel views, it has been demonstrated that it is hard to maintain multi-view consistency [13].

To address this issue, multi-view diffusion has been recently developed [15, 14]. The key idea is jointly to denoise the images for multiple predefined viewpoints conditioned on the same input y, so that a conditional joint distribution of all these views $p_\theta(x_0^{(1)}, \cdots, x_0^{(N)}|y)$ can be learned instead, where N specifies the view number. The forward process adds the same noise to every viewpoint independently at time t, and the reverse process is constructed as:

$$p_\theta(\mathbf{x}_{0:T}^{(1:N)}) = p(\mathbf{x}_T^{(1:N)}) \prod_{t=1}^{T} \prod_{n=1}^{N} p_\theta(\mathbf{x}_{t-1}^{(n)}|\mathbf{x}_t^{(1:N)}), \tag{1}$$

where the per-step per-view denoising is driven by a Gaussian distribution:

$$p_\theta(\mathbf{x}_{t-1}^{(n)}|\mathbf{x}_t^{(1:N)}) = \mathcal{N}(\mathbf{x}_{t-1}^{(n)}; \mu_\theta^{(n)}(\mathbf{x}_t^{(1:N)}, t), \sigma_t^2 \mathbf{I}), \tag{2}$$

with the learnable mean for the n-th view at step t defined as:

$$\mu_\theta^{(n)}(\mathbf{x}_t^{(1:N)}, t) = \frac{1}{\sqrt{\alpha_t}} \left(\mathbf{x}_t^{(n)} - \frac{\beta_t}{\sqrt{1-\bar{\alpha}_t}} \epsilon_\theta^{(n)}(\mathbf{x}_t^{(1:N)}, t) \right), \tag{3}$$

In equation (3), $\epsilon_\theta^{(n)}$ denotes the trainable noise predictor for the n-th view, β_t, specifies the noise schedule, α_t and $\bar{\alpha}_t$ are two scaling constants derived from β_t.

Figure 3: Examples of synthetic face images.

3.2. Gen3D-Face

Extending [1] with prior multi-view diffusion, we take a step towards a generalisable single image 3D face avatar generation, where single unconstrained face images are present without ground-truth mesh. To that end, we first need to address the data scarcity issue as discussed earlier by multi-view face image synthesis for training data augmentation.

3.2.1. Synthetic data preprocessing

We adopt the Panohead [22] to generate additional training images. We generated 25,000 virtual human identities, each represented by 24 images, with azimuth ranging from -180 to 180 degrees. (see Figure 3).

As the synthesis process is not fully controllable, the output quality is often varying [28]. To filter out low-quality face images, we design a pruning process for dealing with the following two issues: (1) *The Janus problem*: We observe cases, where the back-view images present blur faces. To identify such cases, we construct a binary classifier with CLIP using the class names as `back of human head` and `human front face`, and then classify all the back-view face images. We remove those back-view images with the score of the `human front face` class exceeding a threshold τ_{bv}. (2) *Identity inconsistency*: Multi-view face images generated by Panohead [22] are likely to be identity inconsistent. To detect this, we estimate the identity consistency using the average pairwise similarity of views with face embeddings [30] for every individual identity and keep only the top-τ_{ii} virtual identities for model training.

3.2.2. Geometry mesh estimation

To facilitate the 3D face modeling from single images, we integrate the human head mesh [1] as a prior. A key difference in our approach is that we use the mesh estimated from the input image, rather than the ground-truth mesh used in [1]. The reasons are two-fold: (1) Often no ground-truth mesh is available in many real applications; (2) Using ground-truth mesh tends to make the model over rely on this prior, whilst largely ignoring the appearance of the input image. Specifically, we opt for estimating the FLAME mesh $\mathbb{M}$ with v vertices from a single image [31, 32, 33] during both training and inference. This design avoids the need for ground-truth 3D capture, supports privacy-preserving deployment, and as we show in the experiments, effectively prevents the model from overfitting to a fixed mesh template—resulting in better identity preservation and cross-domain generalisation. We also demonstrate that the influence of different estimation methods [31, 32, 33] on the performance can be disregarded.

3.2.3. Multi-view diffusion generation

The key in our context is how to effectively condition the multi-view diffusion process with both the appearance of the single image y and the geometry of the estimated mesh $\mathbb{M}$ (Sec. 3.1).

Specifically, let N noisy target views at time t in our multi-view diffusion process be denoted as $\mathbf{x}_t^{(1:N)}$. To impose viewpoint information, we deploy a CNN encoder to project the camera angles and time embedding to the latent space, which is then added to each novel view's feature embedding $\mathbf{x}_t^{(1:N)}$ respectively. To represent these views in the 3D space, we construct a 3D volume with its vertex $\mathbb{V} \in \mathbb{R}^{L\times L\times L}$ extracted by a linear sampling along each dimension (where L is the number of voxels in each dimension). For each novel view n, we then warp $\mathbb{V}$ according to this view's extrinsic camera parameters, into which the view's feature embedding $\mathbf{x}_t^{(n)}$ is interpolated. This results in an *appearance feature volume* F_a containing N noisy target view features.

To integrate the geometry prior from the estimated mesh $\mathbb{M}$, we adopt a sparse 3D ConvNet [34] to interpolate F_a with $\mathbb{M}$, leading to a *hybrid feature volume* F_{ag} with both appearance and geometry information. The sparse 3D ConvNet [34] is a hierarchical CNN network converting the sparse representation to a dense output tensor. With

F_{ag}, we produce the *view frustum volume* F_{vf} with a light FrustumTV3DNet [15]. This F_{vf} serves as a joint condition for multi-view diffusion by injecting it into the backbone diffusion model (e.g., Stable Diffusion's UNet). The FrustumTV3DNet [15] is a UNet 3D convolutional architecture that processes volumetric input through downsampling stages with time and viewpoint conditioning, followed by skip-connected upsampling paths that return feature maps at multiple resolutions.

As seen from Eq (2), the previous methods [1, 15] store multi-view information by constructing the 3D volume as a condition. To make full use of multi-view information, we propose a ***multi-view joint generation*** algorithm that instead denoises all the views concurrently at one time so that multi-view information interaction can be induced and exploited. Specifically, instead of feeding one view $\mathbf{x}_t^{(n)}$ as the decoder's query at a time, we input sub-views $\mathbf{x}_t^{(1:N)}$ together. This difference enables us to perform the 3D self attention operation [14] among all the novel views $\mathbf{x}_t^{(1:N)}$ and the input y for information exchange and to enhance view consistency.

Model training Our objective function is a multi-view diffusion loss defined as

$$\ell(\theta) = \mathbb{E}_{t,y,c,\mathbf{x}_0^{(1:N)},(1:N),\epsilon^{(1:N)}} \left[\|\epsilon^{(1:N)} - \epsilon_\theta^{(1:N)}(\mathbf{x}_t^{(1:N)}, t)\|_2 \right], \tag{4}$$

where y is the input image, c represents the camera parameters, $\mathbf{x}_0^{(1:N)}$ denotes the N target-view images, $\epsilon^{(1:N)}$ is the added Gaussian noise, and $\epsilon_\theta^{(1:N)}$ is the noise predictor.

4. Experiments

Datasets. We adopt the same train/test split protocol as Morphable Diffusion [1]: 323 identities for training, 36 identities for testing, following the official FaceScape [20] evaluation setting. The same real training data is used for all the models compared, whilst our model also uses synthetic data. For the `out-of-domain` generalised evaluation, we randomly select 1,024 images from FFHQ [35] with the background removed using [36]. We also test on the H3DS dataset [37], which includes multi-view images around the head for 23 identities. For the `in-domain` evaluation, as [1] we use the same 36 test identities in the Facescape dataset [20].

Metrics. For the generalised `out-of-domain` evaluation on **FFHQ** [35], where without access to the multi-view images for each identity, we generate 24 views following the test trajectory from Facescape [20], and evaluate the results using four metrics: (1) Frechet Inception Distance (FID): calculate FID between all input images with all generated images, (2) CLIP Similarity [38]: calculate the similarity between the input image and each generated view across all identities, (3) Input-to-output ID consistency (I2OID): averaging the Arcface cosine similarity [30] between the input image and all generated views, which we propose here to emphasise the importance of identity preservation, (4) Output-to-output ID consistency (O2OID): calculated as the mean of Arcface cosine similarity [30] across all pairs of target views generated from the same input image. We repeat this for the `out-of-domain` dataset **H3DS** [37], which provides captured multi-view images spanning a full 360°. We generate 24 views for each input image, uniformly spaced at 15° intervals from the back to the front. We consider FID, CLIP Similarity and ID consistency between the generated and captured images at matching azimuth angles. Pixel-level metrics are excluded because the captured images include shoulders, hence the head alignment is inconsistent, and after face cropping, the captured image does not exactly match with the generated images.

For conventional `in-domain` evaluation on **Facescape**, following [1], we adopt four metrics: SSIM, LPIPS, FID, and face re-identification accuracy (Re-ID) [39], calculated between the ground truth and the generated images. For the Re-ID metric, we consider two variants: (a) Re-ID(match): As [1], we calculate the match ratio, which is the percentage of cases, where the Euclidean distance between the generated image and the ground truth image falls below the threshold of 0.6. (b) Re-ID(dist): The average Euclidean distance between the generated images and the ground truth images, in addition to the match ratio, which provides the actual distance value to supplement the matching degree.

Implementation. We use the AdamW optimizer with a batch size of 32 for 90k iterations, training for 4 days on two NVIDIA A100 GPUs (80GB each). The learning rate for training the backbone UNet has been raised from 1e-6 to 5e-5 after 100 warm-up steps, and is kept at 5e-4 for all other trainable modules. The inference takes about

Table 1: *Out-of-domain* single image 3D face generation results on FFHQ.

Method	FID↓	CLIP↑	O2OID↑	I2OID↑
Zero-1-to-3 [13]	78.8543	0.5597	0.4483	0.1300
SyncDreamer [15]	68.0294	0.5983	0.4420	0.1572
EG3D [25]	76.1578	0.5142	0.4623	0.1231
PanoHead [22]	58.1578	0.6244	0.4821	0.1611
Morphable Diffusion [1]	66.7443	0.5959	**0.5371**	0.1596
Gen3D-Face (Ours)	**54.9575**	**0.6765**	0.4936	**0.1716**

25 seconds to generate 16 target views from a single input image using 50 DDIM [40] steps on an NVIDIA RTX 3090 GPU. We set $N = 16$ viewpoints, $\tau_{bv} = 0.93$ for back-view image filtering, and $\tau_{ii} = 70\%$ for identity consistency filtering.

Competitors. We compare extensively with existing nerf-based methods, namely pixelNeRF [23], SSD-NeRF [41], and diffusion models including Era3D [42], Zero-1-to-3 [13], SyncDreamer [15], Morphable Diffusion [1], and GAN-based methods EG3D [25] and our data generator PanoHead [22]. Under the proposed `out-of-domain` setting, we exclude pixelNeRF [23] and SSD-NeRF [41] due to providing no precise camera parameters as required, and improve the generalisation of Morphable Diffusion [1] by using the FLAME [43, 33] meshes obtained by fitting the ground truth 3D keypoints, (originally using ground truth bilinear meshes), otherwise it completely falls apart. All methods are fine-tuned on in-domain training data except Era3D [42], which claims good generalization to human heads, and we do not quantitatively evaluate Era3D [42], as it only generates 6 views.

Table 2: *Out-of-domain* single image 3D face generation result on H3DS.

Method	FID↓	CLIP↑	ID Consistency↑
Zero-1-to-3 [13]	77.1547	0.7612	0.1412
SyncDreamer [15]	70.1542	0.7814	0.1652
EG3D [25]	180.1254	0.6014	0.1121
PanoHead [22]	61.2484	0.8246	0.1811
Morphable Diffusion [1]	175.6225	0.7493	0.0977
Gen3D-Face (Ours)	**59.1536**	**0.8453**	**0.1978**

4.1. Evaluation

Out-of-domain evaluation. From the **quantitative** results in Table 1 and Table 2, we observe that: **(1)** Interestingly, the diffusion model with head geometry guidance [1] does not outperform generic object diffusion models (Zero-1-to-3 [13], SyncDreamer [15]) after fine-tuning, nor earlier GAN models (PanoHead [22]) on three out of four metrics in unseen domains. Its performance further degrades when the generation spans a full 360° range of views (Table 2). This suggests that the effectiveness of imposing human geometry in a limited size is constrained. In contrast, our proposed synthetic dataset can improve this limitation. **(2)** The GAN model used to create our synthetic dataset achieves the second-best performance when generating multi-view images without large elevation angles (Table 2). However, its advantage becomes less clear when views include larger elevation angles, as shown in Table 1. Note that EG3D [25] yields almost the worst results because its mainly designed for limited views. **(3)** Overall our Gen3D-Face is the best performer, except being second to Morphable Diffusion [1] on the output-to-output ID consistency metric. We note, however, that looking at this metric *alone* is not comprehensive, and even misleading, since it overlooks the divergence of the generated images from the input (e.g., being consistent multi-view images of a totally different identity). Instead, we should jointly consider both input-to-output and output-to-output ID consistency.

The **qualitative** evaluation is presented in Figure 4, Figure 5 and Figure 9, Figure 5

Figure 4: Novel-view generation results in the out-of-domain setting. **Input**: a single unconstrained FFHQ image (first column). **Generated target views**: rendered using FaceScape test camera poses (except for Era3D, which can only generate six fixed views). Our method produces more 3D-consistent and identity-preserving results than baselines under large viewpoint changes.

Figure 5: Novel-view reconstruction on H3DS (*out-of-domain setting*). **Input**: the frontal H3DS image (middle column). **Generated views**: multi-pose renderings compared against ground-truth views uniformly sampled across 360°. Our method better preserves facial identity and geometric structure across large viewpoint variations than prior methods.

only contain the best performance methods due to the page limit. We attempt to present consistent camera views across the methods within each row, but slight differences remain due to variations in the training camera parameters across the methods, especially for Era3D [42]. We make these observations: **(1)** Zero-1-to-3 [13] tends to produce cartoon style images; **(2)** Era3D [42], the most recent single-image-to-3D method, can only generate six views and exhibits unrealistic geometry; **(3)** SyncDreamer [15] and Morphable Diffusion [1] struggle in preserving the identity; **(4)** Morphable Diffusion [1] generates images that are more consistent, but it suffers from overfitting to the training domain (e.g., added hat for all cases); **(5)** EG3D [25] and Panohead [22] tends to yield more blurry images, especially the face edge, despite taking 20× more training

time, which is caused by the PTI inversion [44]; **(6)** Our Gen3D-Face achieves the overall best result in terms of ID preservation and consistency, and wider pose variation.

Table 3: *In-domain* single image 3D face generation result on Facescape.

Method	SSIM↑	LPIPS↓	FID↓	Re-ID (match)↑	Re-ID (dist)↓
pixelNeRF [23]	0.7898	0.2200	92.61	0.9746	0.3912
Zero-1-to-3 [13]	0.5656	0.4248	10.97	0.9677	0.4193
SSD-NeRF [41]	0.7225	0.2225	34.88	0.9874	0.3855
SyncDreamer [15]	0.7732	0.1854	**6.05**	0.9960	0.3391
PanoHead [22]	0.7871	0.1914	7.10	0.9915	0.3412
Morphable Diffusion [1]	**0.8064**	**0.1653**	6.73	**0.9986**	**0.3372**
Gen3D-Face	0.7995	0.1701	6.1231	0.9981	0.3375

In-domain evaluation. While this work stresses the importance of the out-of-domain generalisation, we still evaluate the conventional in-domain setting. From Table 3 we observe that our method performs on par with the previous model, Morphable Diffusion [1]. This suggests that our model does not sacrifice the training domain performance, while enhancing the model generalisation. The qualitative evaluation in Figure 6 shows that our method preserves the identity well.

4.2. Ablation studies

Data pruning We show examples of the Janus problem and Identity inconsistency in Figure 7, which are filtered out using our pruning process. The effect of pruning is shown in Table 4.

The training data We evaluate the effect of synthetic and real training data. As shown in Table 5, we find that (1) both real and synthetic data contribute positively, but real data is more useful, despite its smaller size. However, the high output-to-output ID consistency suggests overfitting to the training domain. (2) Relying solely on synthetic

Figure 6: Novel-view generation results on FaceScape in the *in-domain setting*. **Input**: a single FaceScape image. **Generated views**: novel multi-angle renderings compared with those produced by baseline methods under the same viewpoint settings. This suggests that our model does not sacrifice performance in the training domain, while enhancing generalisation ability.

data introduces a domain gap when testing on real images. (3) Using both significantly boosts performance, validating our motivation for the training data augmentation by synthesis.

The mesh prior effect We evaluate the impact of different mesh priors on the generative model for the following scenarios: (1) Mesh estimated using RingNet [31] (2)

Table 4: Effect of pruning synthetic training data - Filtering out synthetic training data with the Janus problem or identity inconsistencies enhances training performance.

Pruning	FID↓	CLIP↑	O2OID↑	I2OID↑
✗	57.3138	0.6624	0.4451	0.1659
✓	**54.9575**	**0.6765**	**0.4936**	**0.1716**

Figure 7: The Janus problem and identity inconsistency with the synthetic data.

Mesh estimated using DECA [32] (3) Mesh estimated using MICA [33] As shown in Table 6, different methods of estimating the mesh from the input image do not significantly affect the generated results.

In Figure 8, we also evaluate training with a ground-truth bilinear mesh [1] and the input-estimated Flame mesh [32] as proposed in our work. We provide different input images and the same mesh (randomly chosen from the Facescape testset), we observed that training with the ground-truth mesh leads to the challenge of preserving the input identity and appearance information from the image. It will more relying on the input mesh, as we can see in Figure 8 (a), even input different images, the generated multi-view images will show similar identity features. In contrast, our solution can let the model also pay attention to the input image, as more specific identity information will come from input image.

Joint multi-view generation We evaluate the effect of our joint multi-view generation in Table 7. Increasing the views cardinality (as shown in Figure 2) requires more train-

Table 5: Effect of training data (real, synthetic, or both) on FFHQ.

Training data	FID↓	CLIP↑	O2OID↑	I2OID↑
Real only	64.2882	0.6110	**0.5217**	0.1618
Synthetic only	85.5801	0.5149	0.4155	0.1011
Both	**54.9575**	**0.6765**	0.4936	**0.1716**

Table 6: Impact of mesh estimation by different methods on a single image on FFHQ. We show that this component is not sensitive.

Method	FID↓	CLIP↑	O2OID↑	I2OID↑
RingNet [31]	53.4471	0.6712	0.4912	0.1713
DECA [32]	54.9575	0.6765	0.4936	0.1716
MICA [33]	54.9812	0.6755	0.4922	0.1716

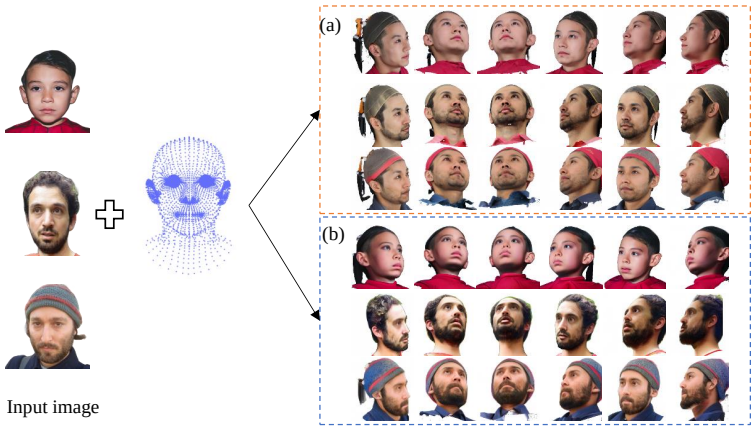

Figure 8: Model trained on different geometry priors: (a) Ground-truth fitted mesh [1]; (b) Our input-estimated mesh. After training, if given different input images with the same mesh, the model trained with (a) tends to generate similar identities despite different inputs. In contrast, the model trained on (b) preserves more distinct identity features from each image.

Table 7: The effect of multi-view joint generation (MVJG). We increase the batch size (maintaining the same iteration count) which reduces epochs when number of views increase, and the results will decrease as views increase because of under-trains. Although more training might help, we fix four views to manage costs.

Number of views	batch size	FID↓	CLIP↑	O2OID↑	I2OID↑
1	70	58.4648	0.6181	0.4441	0.1571
4	28	**54.9575**	**0.6765**	**0.4936**	**0.1716**
8	8	62.1981	0.5541	0.4122	0.1341
16	4	66.4711	0.5344	0.4013	0.1249

ing resources due to the attention module. To balance this, we reduce the batch size when the subset number goes up. Because we keep the same number of training iterations across all configurations, higher subset numbers inevitably lead to less complete training. While longer training could improve performance, we set the view cardinality to four to manage the cost of training in all experiments.

5. Limitations

Our work aims to generate multi-view images from any input image and subsequently perform reconstruction. However, the diffusion-based pipeline requires multiple denoising steps per view, resulting in high computation and limiting real-time deployment. Additionally, performance may drop under extremely exaggerated expressions or challenging pose combinations, as input-estimated FLAME meshes and the training data provide limited coverage of such rare geometric deformations, leading to less reliable conditioning. Also due to the relatively narrow distribution of camera intrinsics in our training data and the current assumption of a fixed focal length in the 3D feature projection, our method can be sensitive to focal-length variations in the input image, which may lead to geometric distortions in novel views. Moreover, occlusions or facial decorations (e.g., hands, microphones, large glasses, heavy makeup) remain challenging, as these patterns are under-represented in the training data and can negatively impact mesh estimation and identity embedding reliability.

6. Conclusion

In this work, we presented a pioneering investigation of the problem of single image 3D face generation in unconstrained, out-of-domain scenario. Built on the recent multi-view diffusion approach, we proposed a novel generative method, Gen3D-Face, that generates photorealistic 3D human face avatars from single, unconstrained images. To achieve this, Gen3D-Face integrates three key components: (i) a hybrid real-and-synthetic training pipeline with quality-controlled augmentation to enhance cross-domain generalisation, (ii) a joint multi-view diffusion scheme that enforces cross-view appearance consistency, and (iii) input-conditioned mesh estimation that provides structural guidance while maintaining flexibility for in-the-wild inputs. Extensive experiments show that our method not only surpasses state-of-the-art baselines in challenging out-of-domain scenarios, but also remains competitive under standard in-domain settings, demonstrating its strong generalisation capability and broad applicability to real-world single-image 3D avatar generation. Looking forward, we plan to reduce computational cost through accelerated sampling, lightweight backbones, or model distillation, enhance robustness to focal-length variation and occlusion through improved camera modelling and occlusion-aware training, and better handle extreme facial expressions and poses by incorporating expression/pose-conditioned training and more diverse geometric priors.

References

[1] X. Chen, M. Mihajlovic, S. Wang, S. Prokudin, S. Tang, Morphable diffusion: 3d-consistent diffusion for single-image avatar creation, in: Proceedings of the IEEE/CVF Conference on Computer Vision and Pattern Recognition, 2024, pp. 10359–10370.

[2] A. Trevithick, M. Chan, M. Stengel, E. R. Chan, C. Liu, Z. Yu, S. Khamis, M. Chandraker, R. Ramamoorthi, K. Nagano, Real-time radiance fields for single-image portrait view synthesis, in: ACM Transactions on Graphics, 2023.

[3] Z. Huang, S. M. Erfani, S. Lu, M. Gong, Efficient neural implicit representation for 3d human reconstruction, Pattern Recognition 156 (2024) 110758.

[4] K. Zeng, Z. Wang, T. Lu, J. Chen, B. Huang, Z. Han, X. Tian, Realistic frontal face reconstruction using coupled complementarity of far-near-sighted face images, Pattern Recognition 129 (2022) 108754.

[5] Y. Hong, B. Peng, H. Xiao, L. Liu, J. Zhang, Headnerf: A real-time nerf-based parametric head model, in: Proceedings of the IEEE/CVF Conference on Computer Vision and Pattern Recognition, 2022, pp. 20374–20384.

[6] B. Xu, J. Zhang, K.-Y. Lin, C. Qian, Y. He, Deformable model driven neural rendering for high-fidelity 3d reconstruction of human heads under low-view settings, arXiv preprint arXiv:2303.13855 (2023).

[7] W. Zielonka, T. Bolkart, J. Thies, Instant volumetric head avatars, in: Proceedings of the IEEE/CVF Conference on Computer Vision and Pattern Recognition, 2023, pp. 4574–4584.

[8] S. Qian, T. Kirschstein, L. Schoneveld, D. Davoli, S. Giebenhain, M. Nießner, Gaussianavatars: Photorealistic head avatars with rigged 3d gaussians, in: Proceedings of the IEEE/CVF Conference on Computer Vision and Pattern Recognition, 2024, pp. 20299–20309.

[9] L. Zhang, Q. Qiu, H. Lin, Q. Zhang, C. Shi, W. Yang, Y. Shi, S. Yang, L. Xu, J. Yu, Dreamface: Progressive generation of animatable 3d faces under text guidance, arXiv preprint arXiv:2304.03117 (2023).

[10] X. Han, Y. Cao, K. Han, X. Zhu, J. Deng, Y.-Z. Song, T. Xiang, K.-Y. K. Wong, Headsculpt: Crafting 3d head avatars with text, in: Thirty-seventh Conference on Neural Information Processing Systems, 2023.

[11] R. Rombach, A. Blattmann, D. Lorenz, P. Esser, B. Ommer, High-resolution image synthesis with latent diffusion models, in: Proceedings of the IEEE/CVF conference on computer vision and pattern recognition, 2022, pp. 10684–10695.

[12] B. Poole, A. Jain, J. T. Barron, B. Mildenhall, Dreamfusion: Text-to-3d using 2d diffusion, arXiv preprint arXiv:2209.14988 (2022).

[13] R. Liu, R. Wu, B. Van Hoorick, P. Tokmakov, S. Zakharov, C. Vondrick, Zero-1-to-3: Zero-shot one image to 3d object, in: Proceedings of the IEEE/CVF international conference on computer vision, 2023, pp. 9298–9309.

[14] Y. Shi, P. Wang, J. Ye, L. Mai, K. Li, X. Yang, Mvdream: Multi-view diffusion for 3d generation, arXiv:2308.16512 (2023).

[15] Y. Liu, C. Lin, Z. Zeng, X. Long, L. Liu, T. Komura, W. Wang, Syncdreamer: Generating multiview-consistent images from a single-view image, arXiv preprint arXiv:2309.03453 (2023).

[16] B. Mildenhall, P. P. Srinivasan, M. Tancik, J. T. Barron, R. Ramamoorthi, R. Ng, Nerf: Representing scenes as neural radiance fields for view synthesis, Communications of the ACM 65 (1) (2021) 99–106.

[17] Y. Wang, Q. Han, M. Habermann, K. Daniilidis, C. Theobalt, L. Liu, Neus2: Fast learning of neural implicit surfaces for multi-view reconstruction, in: Proceedings of the IEEE/CVF International Conference on Computer Vision, 2023, pp. 3295–3306.

[18] B. Kerbl, G. Kopanas, T. Leimkühler, G. Drettakis, 3d gaussian splatting for real-time radiance field rendering, ACM Transactions on Graphics 42 (4) (2023) 1–14.

[19] T. Wang, B. Zhang, T. Zhang, S. Gu, J. Bao, T. Baltrusaitis, J. Shen, D. Chen, F. Wen, Q. Chen, et al., Rodin: A generative model for sculpting 3d digital avatars using diffusion, in: Proceedings of the IEEE/CVF Conference on Computer Vision and Pattern Recognition, 2023, pp. 4563–4573.

[20] H. Yang, H. Zhu, Y. Wang, M. Huang, Q. Shen, R. Yang, X. Cao, Facescape: A large-scale high quality 3d face dataset and detailed riggable 3d face prediction, in: IEEE/CVF Conference on Computer Vision and Pattern Recognition, 2020.

[21] D. Pan, L. Zhuo, J. Piao, H. Luo, W. Cheng, Y. Wang, S. Fan, S. Liu, L. Yang, B. Dai, et al., Renderme-360: A large digital asset library and benchmarks towards high-fidelity head avatars, Advances in Neural Information Processing Systems 36 (2024).

[22] S. An, H. Xu, Y. Shi, G. Song, U. Y. Ogras, L. Luo, Panohead: Geometry-aware 3d full-head synthesis in 360deg, in: Proceedings of the IEEE/CVF Conference on Computer Vision and Pattern Recognition, 2023, pp. 20950–20959.

[23] A. Yu, V. Ye, M. Tancik, A. Kanazawa, pixelnerf: Neural radiance fields from one or few images, in: Proceedings of the IEEE/CVF Conference on Computer Vision and Pattern Recognition, 2021, pp. 4578–4587.

[24] S. Szymanowicz, C. Rupprecht, A. Vedaldi, Splatter image: Ultra-fast single-view 3d reconstruction, in: Proceedings of the IEEE/CVF conference on computer vision and pattern recognition, 2024, pp. 10208–10217.

[25] E. R. Chan, C. Z. Lin, M. A. Chan, K. Nagano, B. Pan, S. De Mello, O. Gallo, L. J. Guibas, J. Tremblay, S. Khamis, et al., Efficient geometry-aware 3d generative adversarial networks, in: Proceedings of the IEEE/CVF Conference on Computer Vision and Pattern Recognition, 2022, pp. 16123–16133.

[26] M. Loper, N. Mahmood, J. Romero, G. Pons-Moll, M. J. Black, Smpl: A skinned multi-person linear model, in: Seminal Graphics Papers: Pushing the Boundaries, Volume 2, 2023, pp. 851–866.

[27] M. Deitke, R. Liu, M. Wallingford, H. Ngo, O. Michel, A. Kusupati, A. Fan, C. Laforte, V. Voleti, S. Y. Gadre, et al., Objaverse-xl: A universe of 10m+ 3d objects, Advances in Neural Information Processing Systems 36 (2024).

[28] Y. Lan, F. Tan, D. Qiu, Q. Xu, K. Genova, Z. Huang, S. Fanello, R. Pandey, T. Funkhouser, C. C. Loy, Y. Zhang, Gaussian3diff: 3d gaussian diffusion for 3d full head synthesis and editing, arXiv (2023).

[29] Y. Deng, D. Wang, X. Ren, X. Chen, B. Wang, Portrait4d: Learning one-shot 4d head avatar synthesis using synthetic data, in: Proceedings of the IEEE/CVF Conference on Computer Vision and Pattern Recognition, 2024, pp. 7119–7130.

[30] J. Deng, J. Guo, N. Xue, S. Zafeiriou, Arcface: Additive angular margin loss for deep face recognition, in: Proceedings of the IEEE/CVF conference on computer vision and pattern recognition, 2019, pp. 4690–4699.

[31] S. Sanyal, T. Bolkart, H. Feng, M. Black, Learning to regress 3D face shape and expression from an image without 3D supervision, in: Proceedings IEEE Conf. on Computer Vision and Pattern Recognition, 2019, pp. 7763–7772.

[32] Y. Feng, H. Feng, M. J. Black, T. Bolkart, Learning an animatable detailed 3D face model from in-the-wild images, in: ACM Transactions on Graphics, Vol. 40, 2021.
URL https://doi.org/10.1145/3450626.3459936

[33] W. Zielonka, T. Bolkart, J. Thies, Towards metrical reconstruction of human faces, in: European Conference on Computer Vision, 2022.

[34] B. Graham, M. Engelcke, L. Van Der Maaten, 3d semantic segmentation with submanifold sparse convolutional networks, in: Proceedings of the IEEE conference on computer vision and pattern recognition, 2018, pp. 9224–9232.

[35] T. Karras, S. Laine, T. Aila, A style-based generator architecture for generative adversarial networks, in: Proceedings of the IEEE/CVF conference on computer vision and pattern recognition, 2019, pp. 4401–4410.

[36] X. Qin, Z. Zhang, C. Huang, M. Dehghan, O. Zaiane, M. Jagersand, U2-net: Going deeper with nested u-structure for salient object detection, in: Pattern Recognition, Vol. 106, 2020, p. 107404.

[37] E. Ramon, G. Triginer, J. Escur, A. Pumarola, J. Garcia, X. Giro-i Nieto, F. Moreno-Noguer, H3d-net: Few-shot high-fidelity 3d head reconstruction, in: Proceedings of the IEEE/CVF International Conference on Computer Vision, 2021, pp. 5620–5629.

[38] A. Radford, J. W. Kim, C. Hallacy, A. Ramesh, G. Goh, S. Agarwal, G. Sastry, A. Askell, P. Mishkin, J. Clark, et al., Learning transferable visual models from natural language supervision, in: International conference on machine learning, PMLR, 2021, pp. 8748–8763.

[39] P. J. Phillips, H. Moon, S. A. Rizvi, P. J. Rauss, The feret evaluation methodology for face-recognition algorithms, IEEE Transactions on pattern analysis and machine intelligence 22 (10) (2000) 1090–1104.

[40] J. Song, C. Meng, S. Ermon, Denoising diffusion implicit models, arXiv preprint arXiv:2010.02502 (2020).

[41] H. Chen, J. Gu, A. Chen, W. Tian, Z. Tu, L. Liu, H. Su, Single-stage diffusion nerf: A unified approach to 3d generation and reconstruction, in: Proceedings of the IEEE/CVF international conference on computer vision, 2023, pp. 2416–2425.

[42] P. Li, Y. Liu, X. Long, F. Zhang, C. Lin, M. Li, X. Qi, S. Zhang, W. Xue, W. Luo, et al., Era3d: high-resolution multiview diffusion using efficient row-wise attention, Advances in Neural Information Processing Systems 37 (2024) 55975–56000.

[43] T. Li, T. Bolkart, M. J. Black, H. Li, J. Romero, Learning a model of facial shape and expression from 4d scans., ACM Trans. Graph. 36 (6) (2017) 194–1.

[44] D. Roich, R. Mokady, A. H. Bermano, D. Cohen-Or, Pivotal tuning for latent-based editing of real images, ACM Transactions on graphics 42 (1) (2022) 1–13.

7. Supplementary

Figure 9: More examples of the novel-view generation results in the out-of-domain setting. Input: a single unconstrained FFHQ image (first column). Generated target views: rendered using FaceScape test camera poses. Our method produces more 3D-consistent and identity- preserving results than baselines under large viewpoint changes.

Table 8: Schematic comparison between our Gen3D-Face and closely related methods.

(a) Gen3D-Face vs Morphable Diffusion

	Gen3D-Face (Ours)	Morphable Diffusion [1]
Model type	Diffusion (latent, multi-view)	Diffusion (latent, multi-view)
Geometry prior	Input-estimated FLAME mesh	GT bilinear head mesh
Mesh requirement	No GT mesh; single-image fitting only	Requires GT mesh for training
Training data	Hybrid real FaceScape + pruned synthetic faces (PanoHead)	Real FaceScape only (limited domain)
Target domain	3D human heads (unconstrained)	3D human heads (in-domain)
Multi-view consistency	Joint multi-view denoising	Per-view denoising
Identity preservation	Strong	Limited, domain overfitting
OOD generalisation	Strong	Weak

(b) SyncDreamer vs PanoHead

	SyncDreamer [15]	PanoHead [22]
Model type	Diffusion (latent, multi-view)	GAN (tri-plane)
Geometry prior	None (generic 3D prior)	None (implicit in tri-plane)
Mesh requirement	No mesh	No mesh
Training data	Generic object 3D datasets	Single View datasets (FFHQ)
Target domain	Generic 3D objects	GAN training domain faces
Multi-view consistency	Synchronized diffusion	No explicit diffusion coupling
Identity preservation	Weak for faces	Need GAN inversion
OOD generalisation	Not specialised for faces	Drops under extreme pose shift

Table 9: Combined ablation results on FFHQ showing the effect of synthesis data pruning, input-estimated mesh prior, and multi-view joint generation. Removing any component leads to noticeable degradation across image fidelity, identity similarity, and multi-view consistency metrics.

Component	FID↓	CLIP↑	O2OID↑	I2OID↑
w/o synthesis data pruning	57.3138	0.6624	0.4451	0.1659
w/o mesh prior	64.0154	0.6083	0.4320	0.1472
w/o multi-view joint generation	58.4648	0.6181	0.4441	0.1571
All	**54.9575**	**0.6765**	**0.4936**	**0.1716**